Eur. Phys. J. B **34**, 163–171 (2003)
DOI: 10.1140/epjb/e2003-00208-2

THE EUROPEAN PHYSICAL JOURNAL B

Synthesis of γ-Fe_2O_3 nanoparticles coated on silica spheres: Structural and magnetic properties

S. Chakrabarti[1], S.K. Mandal[2], B.K. Nath[2], D. Das[2], D. Ganguli[1], and S. Chaudhuri[1,a]

[1] Department of Materials Science, Indian Association for the Cultivation of Science, Kolkata 700 032, India
[2] Inter University Consortium for DAE Facilities, III/LB/8, Bidhan Nagar, Kolkata 700 098, India

Received 9 December 2002 / Received in final form 24 March 2003
Published online 4 August 2003 –

Abstract. The structural and magnetic properties of γ-Fe_2O_3 nanoparticles dispersed on silica spheres prepared by sol-gel method were investigated. The properties of γ-Fe_2O_3 nanoparticles without silica were compared with those on silica spheres. Both the nanoparticle assemblages were characterized by X-ray diffraction (XRD), transmission electron microscope (TEM), Mössbauer (20, 80 and 300 K) and electron paramagnetic resonance (EPR) (80, 300 K) measurements. The XRD spectra clearly indicated the formation of pure γ-Fe_2O_3 nanoparticles and the absence of any other form of iron oxide. TEM images showed a uniform distribution of the nanoparticles of size $\sim$6 nm on the surfaces of silica spheres (diameter $\sim$ 35–60 nm). The size of the individual nanoparticles (without silica) varied within 5–6 nm. The low temperature (20 K) Mössbauer spectra consisted of a partially split sextet superimposed on a doublet. The partial magnetic splitting of the sextet at 20 K revealed the effect of surface magnetization and surface modifications of the γ-Fe_2O_3 nanoparticles coated on silica spheres. The gradual collapse of the partially split sextet into a doublet with increasing temperature indicated the superparamagnetic relaxation exhibited by the γ-Fe_2O_3 nanoparticles with/without silica. The surface magnetization arising out of mis-aligned spins at the surface as evidenced by Mössbauer spectra was further confirmed by electron paramagnetic resonance (EPR) studies.

PACS. 81.20.Fw Sol-gel processing – 76.80.+y Mössbauer effect – 76.30.-v Electron paramagnetic resonance studies

1 Introduction

Finite size effects in nanoparticles or in nanocomposites play an important role in determining their unique electronic, optical and magnetic properties [1–6]. Nanomaterials are characterized by an increased surface to volume ratio compared to the corresponding bulk form. With the reduction in particle size, the surface/interface of nanoparticles gets modified with a new structure due to the appearance of a large number of atoms. This results in a rearrangement of the surface atoms, ions and the electron density distribution at the surface. The surface modification greatly influences the physical properties, in particular the magnetic properties of ultrafine nanocrystals. The surface of the magnetic nanoparticles is found to be in a more disordered state with reduced coordination number and misaligned spins [7–10] compared to the atoms in the bulk. As a consequence, the concept of single domain theory leading to a coherent relaxation of spin magnetic moments loses its significance. The magnetization arising out of the core of the particle differs significantly from that of the surface. The strong exchange interactions between the atoms results in magnetization along the bulk easy axis of magnetization in the core of the particle and the direction changes gradually as the surface is approached. As a result, the total magnetization exhibited by the fine particle system is reduced from its bulk value. To date, several authors [1,7–13] have discussed the effect of surface on the magnetic properties of nanoparticles but the whole mechanism is not yet well understood. Over the years γ-Fe_2O_3 has received much attention because of its magnetic and catalytic [14] properties. It has a dominant role in magnetic storage media such as magnetic tapes [1,15,16]. During the last twenty years, several groups have reported the exciting magnetic and optical properties of γ-Fe_2O_3 nanoparticles embedded in various matrices, particularly in a silica gel matrix [17–21]. However, proper understanding of the magnetic properties of nanoparticles, especially the relationship between magnetism and nanostructure is still not very clear.

Synthesis of phase-pure γ-Fe_2O_3 is rather difficult because the other phases of iron oxides tend to co-crystallize

[a] e-mail: mssc2@mahendra.iacs.res.in

easily. However, for fruitful exploitation of its various magnetic and catalytic properties it is necessary to synthesize it in a pure form. Instead of embedding γ-Fe_2O_3 nanoparticles in silica matrix, We have synthesized individual γ-Fe_2O_3 nanoparticles and nanoparticles dispersed *in situ* on sol-gel silica spheres. The γ-Fe_2O_3 nanoparticles with and without silica spheres are referred to as pure γ-Fe_2O_3 and γ-Fe_2O_3/silica respectively.

2 Experimental details

γ-Fe_2O_3 nanoparticles and the same dispersed on silica spheres were prepared in the following way. Before discussing the details of the synthesis procedure of γ-Fe_2O_3 it seems necessary to point out the crystal structural characteristics of γ-Fe_2O_3 and the rationale behind the selection of the two salt precursors of iron. γ-Fe_2O_3 belongs to the spinel family of structures (AB_2O_4, with tetrahedral A sites and octahedral B sites). Due to the fact that Fe^{3+} prefers tetrahedral coordination, the task of forming a spinel structure is not fulfilled by the availability of only Fe^{3+} in the reaction medium. Therefore addition of a Fe^{2+} salt is necessary as Fe^{2+} prefers octahedral sites. After the formation of the spinel structure in the solution, subsequent oxidation leads to the formation of γ-Fe_2O_3 with spinel structure.

2.1 Preparation of γ-Fe_2O_3 nanoparticles

Salts of both ferrous and ferric ions were used in the synthesis procedure. The source of Fe^{2+} ion was $FeSO_4$, $7H_2O$ and that of Fe^{3+} ion was $FeCl_3$ anhydrous. For the desired precipitation of γ-Fe_2O_3, $FeSO_4 \cdot 7H_2O$ and $FeCl_3$ were taken in the molar ratio of 1:2. NH_4OH solution (25%) was added to the aqueous solution of ferrous sulphate and ferric chloride dropwise, until the pH of the solution became 11. The molar ratio of $FeSO_4$, $7H_2O$: $FeCl_3$: H_2O was 1:2:1210. A black precipitate was produced instantly. This precipitate was acidified to pH=3 by addition of (10.8 N) HCl. After acidification the black precipitate turned brown in colour, indicating the formation of γ-Fe_2O_3 [22].

2.2 Preparation of silica particles coated with γ-Fe_2O_3 nanoparticles

A composite of iron oxide and silica with molar ratio 10:90 was prepared. Here a base catalyst was used in preparing silica sol.

The silica part was prepared using Tetraethyl Orthosilicate (TEOS) dissolved in ethanol followed by the addition of water under stirring. The molar ratio of TEOS: C_2H_5OH: H_2O was 1:17:4.5. After 15 minutes of stirring, NH_4OH solution (25%) was added to the sol dropwise until the pH of the sol became > 10. As the pH of the sol reached this value rapid polymerization started and the transparent sol became colloidal [23,24] within 10 minutes of stirring. On the other hand an aqueous solution of $FeSO_4$, $7H_2O$ and $FeCl_3$ was simultaneously prepared with a molar ratio of $FeSO_4$, $7H_2O$: $FeCl_3$: H_2O = 1:2:1210. When the silica sol became slightly turbid, the aqueous solution of iron salts was poured into the silica sol and mixed under continuous stirring. During the stirring the pH of the slurry dropped to 0.08 then the value of pH was raised to $\sim$3 after 1 h stirring with the addition of a few drops of NH_4OH solution (25%). Finally after another 1 h stirring the precipitate was collected and dried at 100 °C for 1/2 h. Both the products were examined under TEM.

2.3 Measurements

The crystal structure of the particles was investigated using a Rich Seifert S-3000P X-ray diffractometer (XRD). The particle size and morphology were observed with a Hitachi H-600 transmission electron microscope (TEM).

The Mössbauer spectra were recorded in transmission geometry using a conventional spectrometer with 1024 channels operating in constant acceleration mode. A 10 mCi Co^{57} in Rh matrix was used as radioactive source. The spectrometer was calibrated with a high purity 12 μm natural iron foil. Low temperature spectra were recorded by mounting the sample in the optical shroud of a closed cycle helium refrigerator (CCS 850, Janis Research Inc.). The spectra were fitted by a least squares fit program [25] assuming a Lorentzian line shape.

The EPR measurements were carried out with a Varian X-band E-109 century series spectrometer equipped with a variable temperature cryostat.

3 Results and discussion

3.1 Results

In the present work our aim was to study the structural and magnetic properties of the γ-Fe_2O_3 nanoparticles and compare with the corresponding results when the nanoparticles are dispersed on silica spheres and to answer the following questions.

i) What is the difference between pure γ-Fe_2O_3 and γ-Fe_2O_3/SiO_2 in terms of their structural and magnetic properties?
ii) What is the effect of surface magnetization arising out of misaligned spin on the magnetic properties exhibited by the both types of nanoparticles?
iii) Considering the nature of the substance and its nanoscopic size do they exhibit superparamagnetic effect?

The TEM image of pure γ-Fe_2O_3 (Fig. 1a) shows a very narrow size distribution (average size $d \sim 6$ nm) of the nanoparticles. Figure 1b depicts the electron microscopic view of the γ-Fe_2O_3 nanoparticles when coated on silica spheres. It clearly indicates a uniform and homogeneous

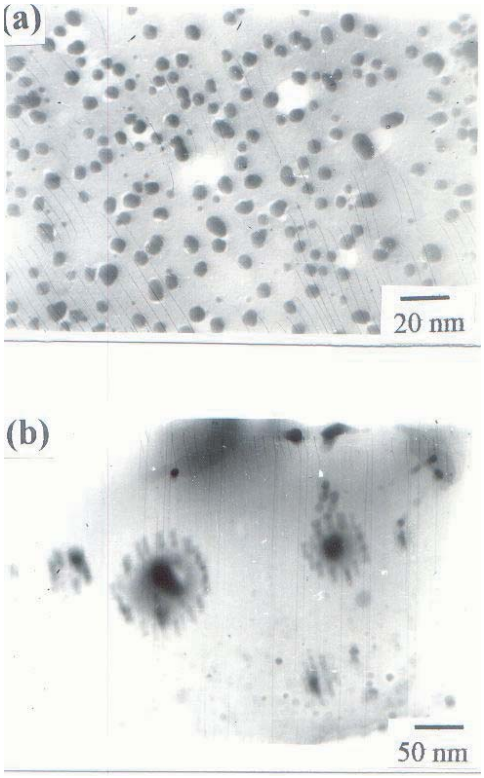

Fig. 1. TEM image of (a) pure γ-Fe_2O_3 nanoparticles and (b) γ-Fe_2O_3 nanoparticles coated on silica spheres respectively.

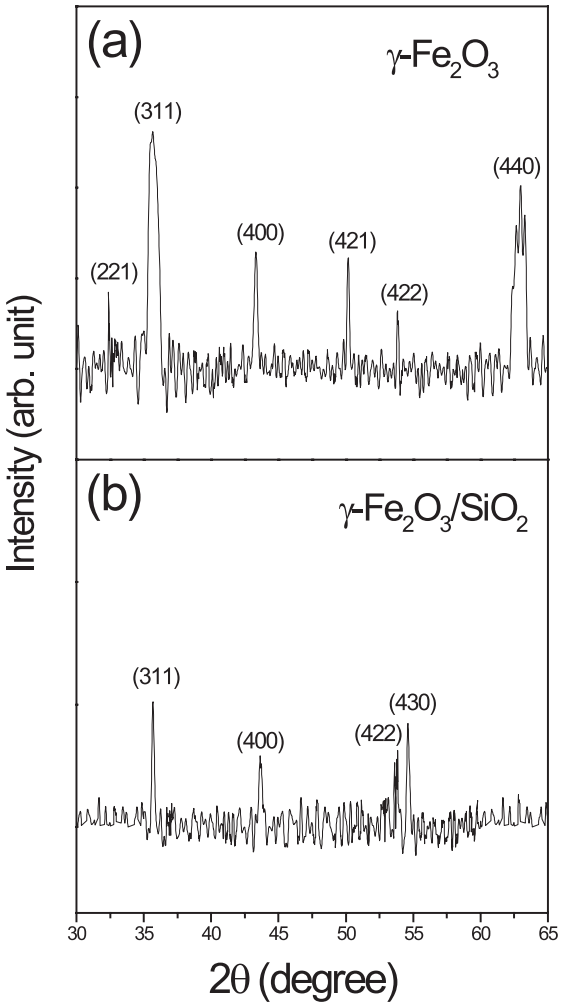

Fig. 2. X-ray diffraction pattern of γ-Fe_2O_3 nanoparticles in powder form.

dispersion. The silica spheres are found to have a distribution in size with diameter $\sim$ 35–60 nm.

The XRD patterns of pure γ-Fe_2O_3 (Fig. 2a) and γ-Fe_2O_3/silica nanoparticles (Fig. 2b) show the crystalline phase of γ-Fe_2O_3 in its pure form. γ-Fe_2O_3 nanoparticles after coating on silica spheres led to the suppression of some peaks, *e.g.* (221) and (421) in the XRD pattern compared to pure γ-Fe_2O_3 nanoparticles. Figure 2b also rules out any formation of iron silicate phases.

We carried out ^{57}Fe Mössbauer measurements in the temperature range of 20 K–300 K in order to determine the structural and magnetic properties of γ-Fe_2O_3 nanoparticles coated on silica spheres. The room temperature spectra of both the samples exhibit distinct broad doublets as shown in Figures 3a and 4a. The doublets are assigned to nanoparticles undergoing superparamagnetic relaxation (discussed later). To obtain a Lorentzian fit to the experimental spectra, we assumed that the total absorbance arises from the Mössbauer nucleii residing at two different sites. For the nanoparticles without silica *i.e.* for pure γ-Fe_2O_3, it is conceived that the atoms residing at the grain boundaries experience a slightly different strength of hyperfine interactions than that of the atoms lying away from the grain boundaries or at the interface between two grains. Similarly, for the γ-Fe_2O_3/silica nanoparticles, the contribution to the hyperfine interaction of the nanoparticles lying in the immediate vicinity of silica surface is supposed to be different from that of particles away from the interface or surface. So we fitted the room temperature doublet spectra with two doublets: i) for particles lying at the grain boundary or just above the silica sphere and ii) for particles lying away from the interface or silica surface. The schematic view of the above model is described in Figure 5. The room temperature (300 K) EPR spectrum of pure γ-Fe_2O_3 nanoparticles shows a single, sharp and symmetric line at $g \sim 2$ (Fig. 6a). With lowering of the measuring temperature down to 80 K, the spectrum shows an additional weak line at $g \sim 4.3$ (Fig. 6b). In contrast, for the γ-Fe_2O_3 nanoparticles coated on silica spheres, the EPR spectra recorded at 300 K (Fig. 6c) and 80 K (Fig. 6d) exhibit both the lines *i.e.* at $g \sim 2$ and $g \sim 4.3$ respectively. For better clarifications of the observed broad signal at $g \sim 2$, we plotted the 2nd derivative spectra of the EPR signals as shown in Figure 7.

3.2 Discussion

Based on the results described above, we discuss here the structural and magnetic behaviours of γ-Fe_2O_3 nanoparticles ($d \sim 6$ nm) coated on silica spheres ($d \sim 35$–60 nm).

Table 1. Hyperfine parameters obtained from Mössbauer spectra at 300 K. Site-I and Site-II refer to the interface/grain boundary and away from the interface respectively.

Sample	Site-I				Site-II			
	IS (mm s^{-1})	QS (mm s^{-1})	FWHM (mm s^{-1})	Rel. abs. area (%)	IS (mm s^{-1})	QS (mm s^{-1})	FWHM (mm s^{-1})	Rel. abs area (%)
Pure γ-Fe_2O_3	0.35	0.99	0.43	49	0.35	0.59	0.35	51
Silica/ γ-Fe_2O_3	0.38	1.10	0.38	39	0.35	0.60	0.39	61

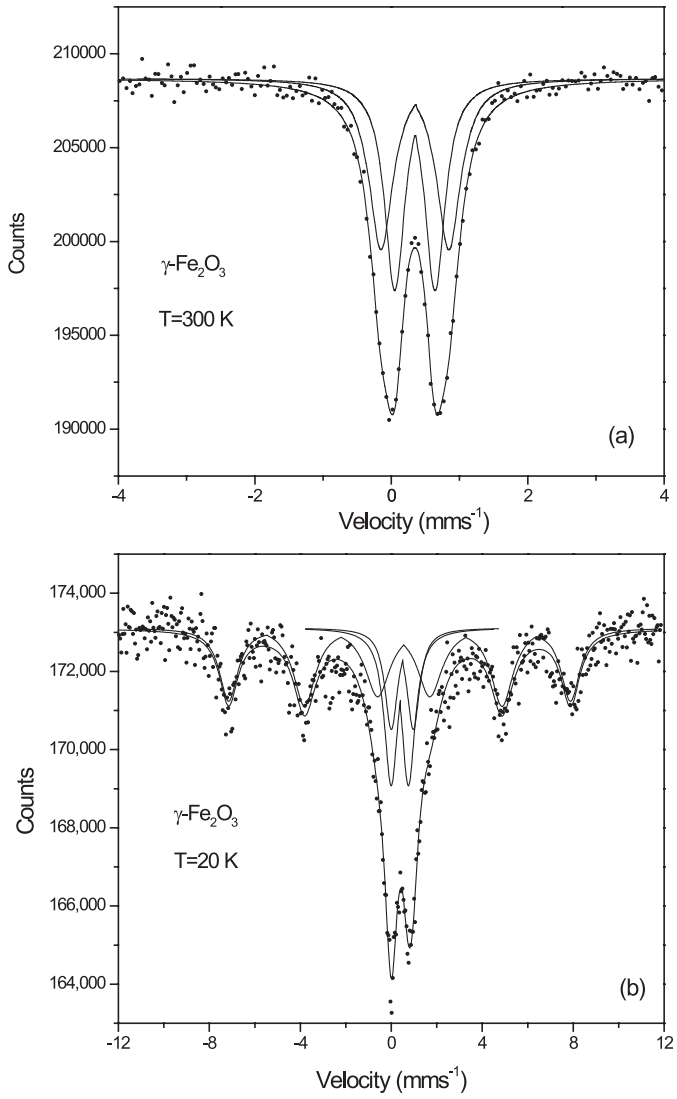

Fig. 3. Mössbauer spectra of pure γ-Fe_2O_3 nanoparticles obtained at (a) 300 K and (b) 20 K respectively. The full lines are fits based on the model as described in the text.

The comments below are made after Mössbauer and EPR spectroscopy studies which are very sensitive for characterizing fine-grained magnetic materials. The parameters obtained from the theoretical fitting of the Mössbauer spectra at 300 K are given in Table 1. The isomer shift (IS) and quadrupole splitting (QS) for the γ-Fe_2O_3/silica and pure γ-Fe_2O_3 nanoparticles did not differ much, as indicated in Table 1. However, the fractional resonance absorption areas of the interfacial part (Site-I) are found to be significantly different in both cases. The reduction in resonance absorption area of the interfacial part of γ-Fe_2O_3/silica nanoparticles indicates a reduction of the number of particles contributing to the resonance absorption. This is expected when the nanoparticles are residing on silica spheres of larger dimensions. It is also observed from Table 1 that there is an appreciable reduction in the linewidth (FWHM) of the resonance absorption for the γ-Fe_2O_3/silica nanoparticles. This narrowing of the linewidth could be ascribed to the possible binding of the nanoparticles to the surface of the silica spheres. The higher the strength of the binding of the nanoparticles to the silica spheres, the higher would be the effective Debye temperature causing narrower linewidth. In our case, the binding is not strong enough to cause changes in IS and QS but still affects the linewidth for γ-Fe_2O_3/silica nanoparticles compared with that of pure γ-Fe_2O_3 nanoparticles.

The magnetic properties of the nanoparticles are strongly influenced by the superparamagnetic relaxation effect *i.e.* the fluctuation of the magnetization vector among the easy axes of magnetization [26,27] and have been widely studied by Mössbauer spectroscopy [28]. The use of γ-Fe_2O_3 nanoparticles in the field of high density recording media is limited by this superparamagnetic relaxation. The temperature dependence of the superparamagnetic relaxation time for a non-interacting and uniaxial magnetic anisotropy nanoparticle system is expressed by [27–29]:

$$\tau = \tau_0 \exp\left(\frac{\Delta E}{k_B T}\right) \tag{1}$$

where k_B is Boltzmann's constant and T is temperature. ΔE is the energy barrier between the two easy directions of magnetization. The pre-exponential factor τ_0 is called the characteristic time which is of the order of 10^{-10}–10^{-12} s and has a weak dependence on temperature [29]. For a distribution in particle size, there will be a distribution of relaxation time and hence in blocking temperature (T_B). In the light of the above discussion, we analyze the Mössbauer spectra of γ-Fe_2O_3 nanoparticles obtained at different temperatures.

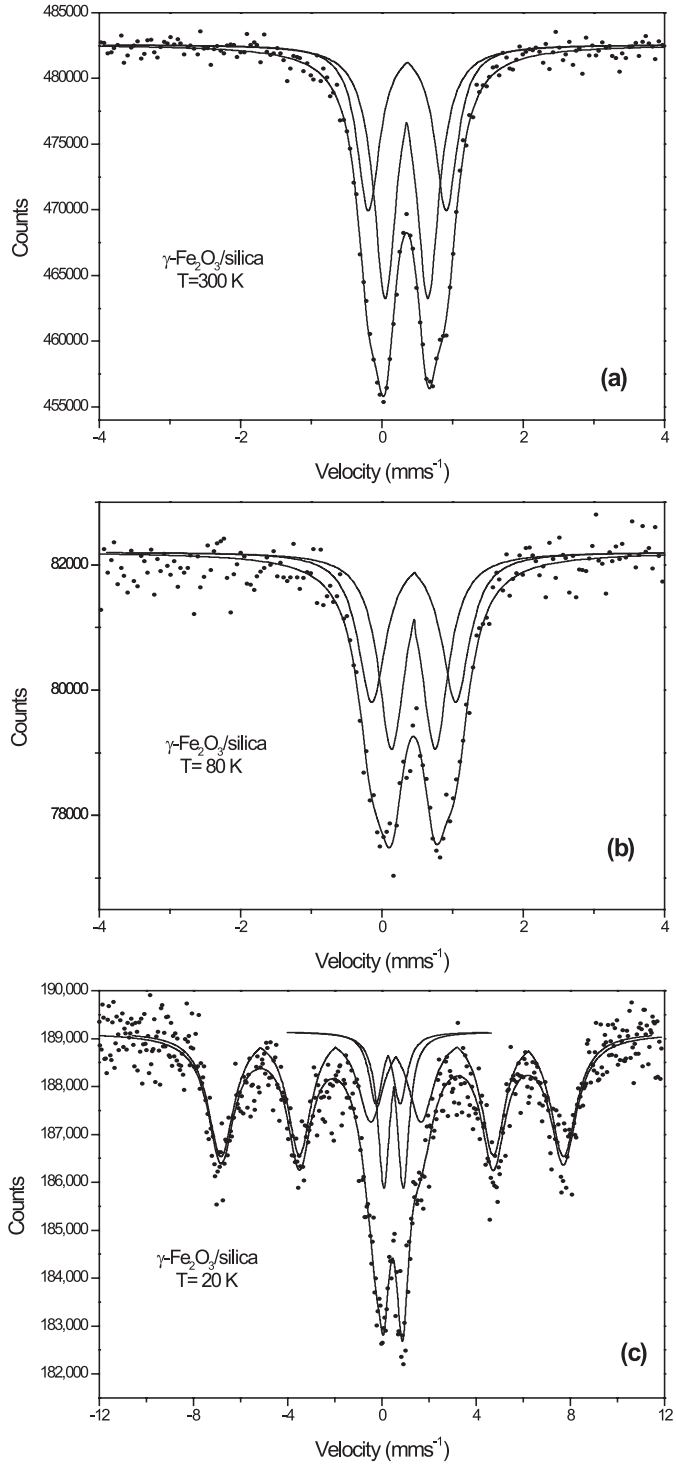

Fig. 4. Mössbauer spectra of γ-Fe_2O_3/silica nanoparticles obtained at (a) 300 K, (b) 80 K and (c) 20 K respectively. The full lines are fits based on the model as described in the text.

The Mössbauer spectrum obtained at 80 K (Fig. 4b) for γ-Fe_2O_3/silica nanoparticles showed the same superparamagnetic relaxation behaviour as exhibited by γ-Fe_2O_3 nanoparticles at 300 K, both showing a quadrupole split doublet. With lowering in temperature down to 20 K, the spectra for both the samples indicated a partial ordering of the doublet into a magnetically split sextet superimposed on a doublet, as indicated in Figures 3b and 4c. The doublet indicated incomplete ferrimagnetic ordering of the γ-Fe_2O_3 nanoparticles at 20 K. The incomplete magnetic ordering could be due to two possible reasons: the presence of very small crystallites, and the spin canting effect [7,30]. The doublet corresponds to a fraction of very small nanocrystallites which are still undergoing superparamagnetic relaxation even at 20 K. In that case, the sample is supposed to contain a distribution in size which translates into a distribution in blocking temperature (T_B).

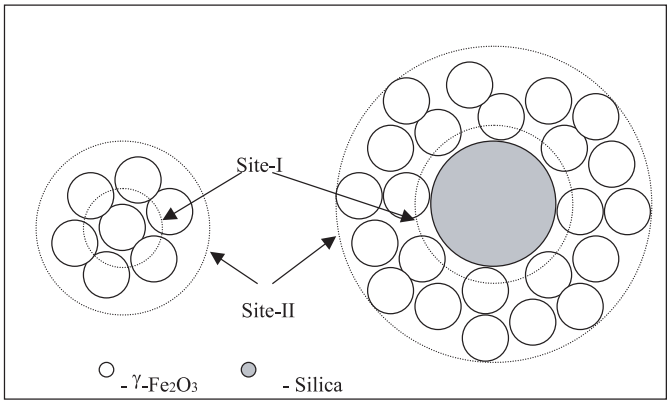

Fig. 5. Schematic view of the model of the arrangement of γ-Fe_2O_3 nanoparticles with and without silica spheres considered for the analysis of Mössbauer spectra.

Another possibility is the spin canting effect *i.e.* the gradual canting of spins from the surface to core of the nanoparticles which results in incomplete magnetic ordering at 20 K. Using Monte Carlo simulations, Iglesias *et al.* [12] found that even at $T = 0$ K, the surface magnetization does not attain perfect magnetic order for γ-Fe_2O_3 nanoparticles with particle size 6.6 nm. We could not rule out either of these two possibilities. It is also worthwhile to mention here that interaction among the particles can affect the superparamagnetic relaxation time and hence the blocking temperature [31–33].

The average hyperfine field at 20 K obtained from the Mössbauer spectra for the magnetically split components of γ-Fe_2O_3/silica and pure γ-Fe_2O_3 nanoparticles are 452 kOe and 466 kOe respectively. The values obtained are lower than that of bulk maghemite and are consistent with the usual observation for nanoparticles [34,35]. Assuming the nanoparticles to be spherical in shape, the hyperfine field (H_T) obtained at the blocking temperature is related through the particle size (d) by [36]:

$$H_T = H_0 \left(1 - \frac{3k_BT}{\pi K d^3}\right) \qquad (2)$$

with H_0 being the hyperfine field at 0 K, and K is the magnetic anisotropy constant. Using $K = 4.7 \times 10^3$ Jm^{-3}, we obtained the particle size for pure γ-Fe_2O_3 and γ-Fe_2O_3/silica nanoparticles to be $\sim$ 6.45 nm and 6.33 nm respectively. This indicated a very similar particle size distribution for the pure γ-Fe_2O_3 and γ-Fe_2O_3/silica

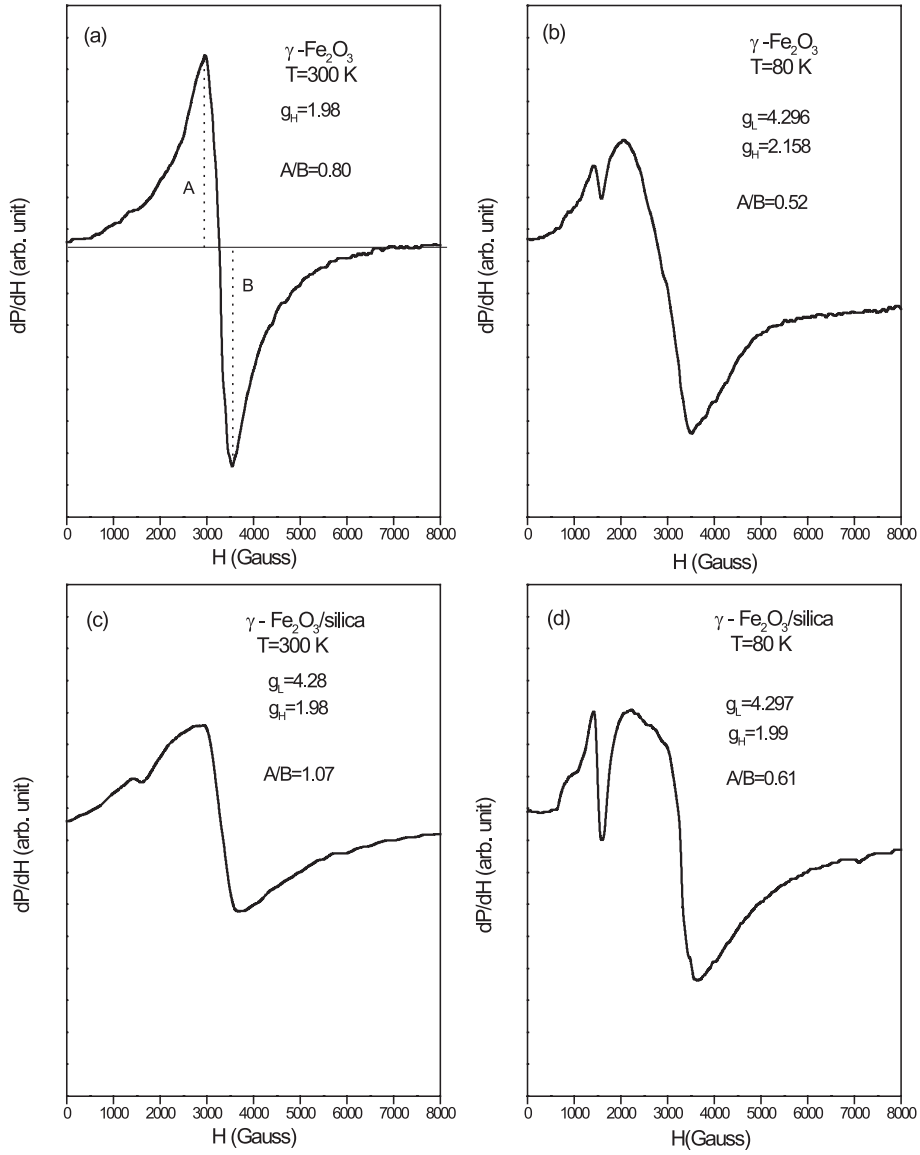

Fig. 6. X-band EPR spectra of pure γ-Fe_2O_3 nanoparticles at (a) 300 K; (b) 80 K and those of γ-Fe_2O_3/silica nanoparticles at (c) 300 K; (d) 80 K respectively.

nanoparticles. Note that we have used here the bulk value of K (magnetic anisotropy constant), though this value has been found to increase due to size and surface effects [35]. The values of particle size obtained from above formulation are consistent with those obtained from transmission electron microscopy (TEM).

To elucidate further the correlation of magnetic properties and electronic structure, we studied the electron paramagnetic resonance (EPR) of pure γ-Fe_2O_3 and γ-Fe_2O_3/silica nanoparticles the results of which are presented in Figure 6. The EPR spectra are displayed as a plot of 1st derivative of the absorbed radiation (dP/dH) with the strength of magnetic field (H). The EPR spectra are found to have a drastic dependence on temperature. Before we explain the EPR results obtained for γ-Fe_2O_3 nanoparticles with and without silica spheres we list below the main features obtained:

i) The existence of an additional weak line at $g \sim 4.3$ at 80 K, in contrast to the appearance of a single line at $g \sim 2$ at 300 K for pure γ-Fe_2O_3 nanoparticles.
ii) The existence of both lines for γ-Fe_2O_3/silica nanoparticles at 300 K as well as at 80 K. The intensity of the signal at $g \sim 4.3$ increased sharply with the decrease in temperature.
iii) The line width of the EPR signal at $g \sim 2$ increased markedly with the decrease in temperature. Also the overall shape of the EPR spectra (defined by the asymmetry parameter A/B (Fig. 6a) became more asymmetric with reduction in temperature for both samples.

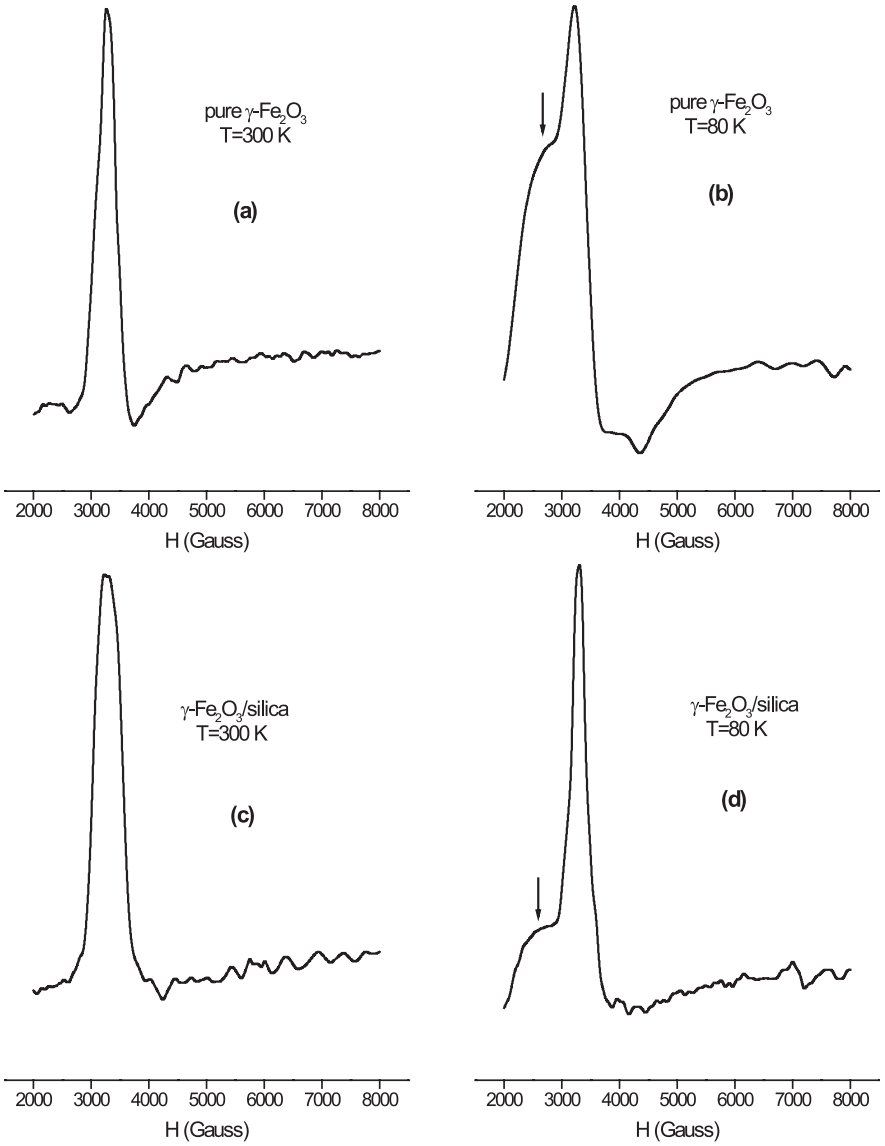

Fig. 7. Second derivative of the EPR spectra for γ-Fe_2O_3 nanoparticles at (a) 300 K; (b) 80 K and those of γ-Fe_2O_3/silica nanoparticles at (c) 300 K; (d) 80 K respectively.

iv) The g values also showed a slight increase with the decrease in temperature.

The origin of the EPR signal at $g \sim 2$ is explained by different authors for Fe_2O_3 and Fe_2O_3-SiO2 system [37–41]. While Jitianu *et al.* [38] thought the peak originated from iron in the polymeric chain: -O-Si-O-Fe-O-Si-O-, Tanaka *et al.* [41] regarded it to be due to Fe^{3+} ions in spin pair of Fe^{3+}-O^2-Fe^{3+}. In our case, any formation of-O-Si-O-Fe-O-Si-O-chains could be ruled out from the Mössbauer and XRD measurements. We ascribe the EPR signal at $g \sim 2$ exhibited by both samples at all temperatures to the superparamagnetic behavior of the iron oxide nanoparticles. The single narrow line at 300 K (Fig. 7a and Fig. 7c) for both samples is associated with the nanoparticles undergoing superparamagnetic relaxation as observed by Mössbauer spectroscopy. However, with the decrease in temperature, the sharp line is found to have an additional broad shoulder at lower field (marked by arrow). This broad line could be ascribed to the fraction of the nanoparticles blocked in the magnetic field with the decrease in temperature. Also, it is evident from the Figures 7b and 7d that the fraction of the particles blocked at 80 K was higher for pure γ-Fe_2O_3 nanoparticles than that of γ-Fe_2O_3/silica nanoparticles. This could be attributed to the effect of surface anisotropy as discussed earlier. The effect of surface anisotropy is more pronounced for the γ-Fe_2O_3/silica nanoparticles than for pure γ-Fe_2O_3 nanoparticles due to the presence of the silica/nanoparticle interface and rearrangement of the particles over the silica sphere. This suggests that at a particular temperature there will be a state comprising both blocked and unblocked fractions (undergoing superparamagnetic relaxation) of the particles. The blocked fraction

will be higher for pure γ-Fe_2O_3 nanoparticles than that for γ-Fe_2O_3/silica nanoparticles. It is to be mentioned here that although EPR evidenced a fraction of the nanoparticles that are blocked at 80 K, no such signal was found from the Mössbauer studies. This discrepancy could be resolved if we consider the characteristic measuring time of EPR and Mössbauer spectroscopy. The typical characteristic measuring time for EPR ($\sim 10^{-9}$ sec) is lower than that of for Mössbauer spectroscopy ($\sim 10^{-8}$ sec). The typical value of the characterization time for magnetization measurement technique is $\sim$ 100 sec. This gives rise to a different response of the magnetic particles to the external field and hence, results in different blocking temperatures as observed from both spectroscopic measurements. EPR being a faster technique, results in a higher blocking temperature and anisotropy barrier for the same system comprising small particles than the corresponding values obtained from magnetization and Mössbauer measurements [42,43].

Now we consider the origin of the observed second signal at $g \sim 4.3$ with a strong thermal dependence of its intensity. The most commonly accepted assignment of this signal is due to Fe^{3+} iron; however, this has been found to be inconsistent with other measurements by several authors [19,37,44]. In our case, this signal at $g \sim 4.3$ could be assigned to the distorted tetrahedral/orthorhombic lattice sites at the surface which has been reported by many authors [19,37]. The lower intensity of this signal at 300 K could arise out of the faster spin relaxation. We cannot rule out that the signal is present for pure γ-Fe_2O_3 at 300 K (Fig. 7a), only that it is too weak to be observed. Furthermore, the slight increase in g values with reduction in temperature suggests the gradual strengthening of the magnetic ordering. As the EPR spectra at 80 K depicted, the ordering is significantly more (marked by arrow in Fig. 7b and Fig. 7d) for the pure γ-Fe_2O_3 nanoparticles than the γ-Fe_2O_3/silica nanoparticles. The obvious reason could be the greater thermal demagnetization of the material due to misalignment of the spins in the latter case. With the reduction in temperature from 300 K to 80 K, the linewidth of the EPR spectra (for $g \sim 2$) changed from $\sim$ 733 to 1466 Gauss for γ-Fe_2O_3 nanoparticles and from $\sim$ 866 to 1400 Gauss for γ-Fe_2O_3/silica nanoparticles respectively. Similar observations on the increase in linewidth with decreasing T were reported earlier for γ-Fe_2O_3 nanoparticles [39] and FeO(OH) [45]. The thermal effect on the overall shape of the EPR spectra as determined by the asymmetry parameter (the ratio of A to B) was also evaluated as shown in Figure 6. A and B are the amplitudes of the signals corresponding to the low and high magnetic fields respectively. The ratio A/B changed from 0.8 to 0.52 for pure γ-Fe_2O_3 nanoparticles and from $\sim$ 1.07 to 0.6 for γ-Fe_2O_3/silica nanoparticles with the decrease in temperature from 300 K to 80 K respectively. It is to be mentioned here that some error is introduced in calculating the A/B ratio due to the mismatch of the baseline in the low and high field regions. Determination of the correct baseline of the overall signal gives an accurate value of the asymmetry parameter [46]. The observed asymmetry at lower temperatures in the EPR line shape indicated the consequences of the thermal effect on the spin relaxation processes involved in magnetic nanoparticles.

4 Conclusions

We have presented here the structural and magnetic properties of both pure γ-Fe_2O_3 nanoparticles and γ-Fe_2O_3 nanoparticles dispersed on silica spheres prepared by sol-gel techniques. The thermal dependence of both the Mössbauer and EPR spectra revealed the effect of structural modifications of the γ-Fe_2O_3 nanoparticles coated on silica spheres. Mössbauer spectroscopy revealed that the incomplete ferrimagnetic ordering at low temperatures was a clear indication of the drastic influence of the surface magnetization on the magnetic properties exhibited by the nanoparticles. EPR spectra also showed line profiles corresponding to the superparamagnetic relaxation of nanoparticles. Detailed results obtained from the thermal dependence of the intensity of EPR signals, its linewidth and g-values were also correlated with the electronic and magnetic properties of γ-Fe_2O_3 nanoparticles.

References

1. *Magnetic Properties of Fine Particles*, edited by J.L. Dormann, D. Fiorani (North- Holland, Amsterdam, 1992)
2. K. Haneda, Can. J. Phys. **65**, 1233 (1987)
3. C.B. Murray, C.R. Kagan, M.G. Wendi, Science **270**, 1335 (1995)
4. M.P. Pileni, J. Phys. Chem. B **105**, 3358 (2001)
5. R.D. Shull, J.J. Ritter, A.J. Shapiro, L.J. Swartzendruber, L.H. Bennett, J. Appl. Phys. **67**, 4490 (1990)
6. M.A. Kastner, Phys. Today **46**, 24 (1993)
7. J.M.D. Coey, Phys. Rev. Lett. **27**, 1140 (1971)
8. O. Eriksson, A.M. Boring, R.C. Albers, G.W. Fernando, B.R. Cooper, Phys. Rev. B **45**, 2868 (1992)
9. A.H. Morrish, K. Haneda, J. Appl. Phys. **52**, 2496 (1981)
10. Q.A. Pankhurst, R.J. Pollard, Phys. Rev. Lett. **67**, 248 (1991)
11. R.H. Kodama, A.E. Berkowitz, Phys. Rev. B. **59**, 6321 (1999)
12. O. Iglesias, A. Labarta, Phys. Rev. B **63**, 184416 (2001)
13. H. Kachkachi, A. Ezzir, M. Nogues, E. Tronc, Eur. Phys. J. B **14**, 681 (2000)
14. G. Ennas, A. Musinu, G. Piccaluga, D. Zedda, D. Gatteschi, G. Sangrogorio, J.L. Stanges, G. Concas, G. Spano, Chem. Mater. **10**, 495 (1998)
15. A.E. Berkowitz, in *Nanomaterials: Synthesis, Properties and Applications*, edited by S. Edelstein, R.C. Cammarata (Institute of Physics Publishing, Bristol, 1996); p. 569
16. MRS Bulletin **15**, 31 (1990)
17. T. Yoshio, C. Kawaguchi, F. Kanamaru, K. Takahashi, J. Non-Cryst. Solids. **43**, 12 (1981)
18. T. Lopez, J. Mendez, T. Zamudio, M. Villa, Mater. Chem. Phys. **30**, 161 (1992)
19. C. Cannas, D. Gatteschi, A. Masinu, G. Piccaluga, C. Sangregorio, J. Phys. Chem. B **102**, 7721 (1998)
20. M.P. Morales, M.J. Munoz-Aguado, J.L. Garcia-Placios, F.J. Lazaro, C.C.J. Serna, J. Magn. Magn. Mater. **183**, 232 (1998)

21. S. Ramesh, I. Felner, Y. Koltypin, A. Gedanken, J. Mat. Res. **15**, 944 (2000)
22. N.J. Cherepy, D.B. Liston, J.A. Lovejoy, H. Deng, J.Z. Zheng, J. Phys. Chem. B. **102**, 770 (1998)
23. W. Stöber, A. Fink, E. Bohn, J. Colloid Interface Sci. **26**, 62 (1968)
24. M. Chaterjee, D. Ganguli, Trans. Ind. Ceram. Soc. **45**, 95 (1986)
25. E. von Meerwall, Comp. Phys. Commun. **9**, 117 (1975)
26. A. Slawska-Waniewska, M. Gutowski, H.K. Lachowicz, T. Kulik, H. Matyja, Phys. Rev. B **46**, 14 594 (1992)
27. L. Neel, Ann. Geophys. **5**, 99 (1949)
28. S. Mørup, J.A. Dumesic, H. Topsoe, *Applications of Mössbauer Spectroscopy*, edited by R.L. Cohen Vol. II (Academic, New York, 1980), p. 1
29. W.F. Brown, Jr., Phys. Rev. **130**, 1677 (1963)
30. A.H. Morrish, K. Haneda, J. Magn. Magn. Mater. **35**, 105 (1983)
31. S. Mørup, E. Tronc, Phys. Rev. Lett. **72**, 3278 (1994)
32. S. Mørup, F. Bødker, P.V. Hendriksen, S. Linderoth, Phys. Rev. B **52**, 287 (1995)
33. S. Mørup, M.B. Madsen, J. Franck, J. Villadsen, C.J.W. Koch, J. Magn. Magn. Mater. **40**, 163 (1983)
34. S. Linderoth, M.D. Bentzon, S. Mørup, Nucl. Instrum. Methods Phys. Res. B **76**, 173 (1993)
35. F. Bødker, S. Morup, S. Linderoth, Phys. Rev. Lett. **72**, 282 (1994)
36. S. Mørup, J. Magn. Magn. Mater. **37**, 39 (1983)
37. D. Goldfarb, M. Bernardo, K.G. Strohmaier, D.E.W. Vaughan, H. Thomann, J. Am. Chem. Soc. **116**, 6344 (1994)
38. A. Jitianu, M. Crisan, A. Meghea, H. Rau, M. Zaharescu, J. Mater. Chem. **12**, 1401 (2002)
39. D. Prodan, V.V. Grecu, M.N. Grecu, E. Tronc, J.P. Jolivet, Meas. Sci. Technol. **10**, L-41 (1999)
40. S. Roy, D. Ganguli, J. Non-Cryst. Sol. **195**, 38 (1996)
41. K. Tanaka, K. Kamiya, M. Matsuoka, T. Yoko, J. Non-Cryst. Sol. **94**, 365 (1987)
42. J.L. Dormann, D. Fiorani, E. Tronc, Adv. Chem. Phys. **98**, 283 (1997)
43. R.D. Sánchez, M.A. López-Quintela, J. Rivas, A. González-Penedo, A.J. Garcìa-Bastida, C.A. Ramos, R.D. Zysler, S. Ribeiro Guevara, J. Phys. Cond. Matt. **11**, 5643 (1999)
44. S.E. Dapurkar, P. Sevlam, Mater. Phys. Mech. **4**, 13 (2001)
45. M. Ibrahim, G. Edwards, B. Ganguly, G.P. Huffman, J. Appl. Phys. **75**, 5873 (1994)
46. H. Kodera, J. Phys. Soc. Jpn **28**, 89 (1970)